Article

Structure

Dissecting Dynamic Allosteric Pathways Using Chemically Related Small-Molecule Activators

Highlights

- Allosteric ligand binding is correlated to structural dynamics in a model enzyme
- A widely dispersed allosteric network has been identified
- Catalytic rate enhancement varies with the degree of millisecond flexibility
- Allosteric ligand binding is communicated over a 25-Å distance

Authors

George P. Lisi, Gregory A. Manley, Heidi Hendrickson, Ivan Rivalta, Victor S. Batista, J. Patrick Loria

Correspondence

victor.batista@yale.edu (V.S.B.), patrick.loria@yale.edu (J.P.L.)

In Brief

Lisi et al. use NMR and computational methods to probe the allosteric influence of small-molecule activators. Allosteric activator-induced changes in millisecond motions are responsible for enhancing the catalytic rate at a distant active site. Interestingly the most activating ligand results in the largest degree of motions.

Lisi et al., 2016, Structure *24*, 1–12
July 6, 2016
http://dx.doi.org/10.1016/j.str.2016.04.010

CellPress

Please cite this article in press as: Lisi et al., Dissecting Dynamic Allosteric Pathways Using Chemically Related Small-Molecule Activators, Structure (2016), http://dx.doi.org/10.1016/j.str.2016.04.010

Structure
Article

Dissecting Dynamic Allosteric Pathways Using Chemically Related Small-Molecule Activators

George P. Lisi,[1,4] Gregory A. Manley,[1,4] Heidi Hendrickson,[1] Ivan Rivalta,[2] Victor S. Batista,[1,*] and J. Patrick Loria[1,3,*]
[1]Department of Chemistry, Yale University, New Haven, CT 06520, USA
[2]École Normale Supérieure de Lyon, CNRS, Université Lyon 1, Laboratoire de Chimie UMR 5182, 46, Allée d'Italie, 69364 Lyon Cedex 07, France
[3]Department of Molecular Biophysics & Biochemistry, Yale University, New Haven, CT 06520, USA
[4]Co-first author
*Correspondence: victor.batista@yale.edu (V.S.B.), patrick.loria@yale.edu (J.P.L.)
http://dx.doi.org/10.1016/j.str.2016.04.010

SUMMARY

The allosteric mechanism of the heterodimeric enzyme imidazole glycerol phosphate synthase was studied in detail with solution nuclear magnetic resonance spectroscopy and molecular dynamics simulations. We studied IGPS in complex with a series of allosteric activators corresponding to a large range of catalytic rate enhancements (26- to 4,900-fold), in which ligand binding is entropically driven. Conformational flexibility on the millisecond timescale plays a crucial role in intersubunit communication. Carr-Purcell-Meiboom-Gill relaxation dispersion experiments probing Ile, Leu, and Val methyl groups reveal that the apo- and glutamine-mimicked complexes are static on the millisecond timescale. Domain-wide motions are stimulated in the presence of the allosteric activators. These studies, in conjunction with ligand titrations, demonstrate that the allosteric network is widely dispersed and varies with the identity of the effector. Furthermore, we find that stronger allosteric ligands create more conformational flexibility on the millisecond timescale throughout HisF. This domain-wide loosening leads to maximum catalytic activity.

INTRODUCTION

The functional implications of direct interactions between enzyme and ligand due to electrostatic and hydrophobic contacts are often readily rationalized from structural and kinetic data (Wolfenden and Snider, 2001); however, an understanding of how these binding interactions are propagated to remote sites is often less clear. Nonetheless, an enzyme's ability to leverage the free energy of effector ligand binding to coordinate structural and dynamical changes over long molecular-scale distances is a hallmark of allostery. Given the central role of allostery in a variety of biological processes, including its functional regulation of enzymatic reactions, allostery has been the object of scientific inquiry for decades (Koshland et al., 1966; Monod et al., 1965; Tsai and Nussinov, 2014), and several well-defined structural (Daily and Gray, 2009; Demerdash et al., 2009; Fairman et al., 2011; Laskowski et al., 2009; Popovych et al., 2009), energetic (Hilser, 2010; Hilser et al., 2012; Motlagh et al., 2012, 2014), and dynamic (Bahar et al., 2007; Bakan and Bahar, 2009; Gunasekaran et al., 2004; Ming and Wall, 2005; Popovych et al., 2006; Rivalta et al., 2012; Rousseau and Schymkowitz, 2005; Tzeng and Kalodimos, 2009) models exist to describe this phenomenon. In addition, it has also recently been demonstrated that multiple allosteric models can be operative in a single enzyme (Freiburger et al., 2011, 2014).

The glutamine amidotransferase imidazole glycerol phosphate synthase (IGPS) is an allosteric enzyme that lies at the branch-point of purine and histidine biosynthetic pathways of bacteria, archaea, plants, and fungi (Chaudhuri et al., 2001; Myers et al., 2005; Sinha et al., 2004). IGPS from *Thermatoga maritima* is a 51-kDa heterodimeric complex of HisH (23 kDa) and HisF (28 kDa) enzymes that synchronizes two distinct catalytic reactions in active sites separated by more than 25 Å (Beismann-Driemeyer and Sterner, 2001). HisH catalyzes the hydrolysis of glutamine (Gln) to yield glutamate and ammonia, after which HisF utilizes the newly generated NH_3 in the cyclization of its substrate, N′-[(5′-phosphoribulosyl)formimino]-5-aminoimidazole-4-carboxamide ribonucleotide (PRFAR), as shown in Figure 1. The mechanism of PRFAR cyclization to yield imidazole glycerol phosphate (IGP) and 5-aminoimidazole-4-carboxamide ribonucleotide (AICAR) has been described in detail (Beismann-Driemeyer and Sterner, 2001; Chaudhuri et al., 2001, 2003). PRFAR cyclization is dependent on successful production, sequestration, and translocation of NH_3 that is generated nearly 30 Å from the HisF effector site, and the glutaminase and cyclization reactions are tightly coupled in a 1:1 stoichiometry (Chaudhuri et al., 2001) despite occurring in different enzyme subunits.

In the absence of HisF-bound PRFAR, the rate of Gln hydrolysis in the HisH subunit is negligible (1.2×10^{-3} s^{-1}) (Myers et al., 2003) but PRFAR binding stimulates the glutaminase subunit, enhancing this basal rate of NH_3 production by 4,900-fold. We have previously shown by nuclear magnetic resonance (NMR) spectroscopy that PRFAR binding allosterically activates a network of dynamic amino acid residues in IGPS. This network is significantly different and strengthened compared with apo IGPS (Lipchock and Loria, 2010; Rivalta et al., 2012). Thus, binding of PRFAR to HisF converts the rigid apoenzyme to one that undergoes protein-wide conformational exchange motions on the millisecond timescale (Lipchock and Loria, 2009, 2010).

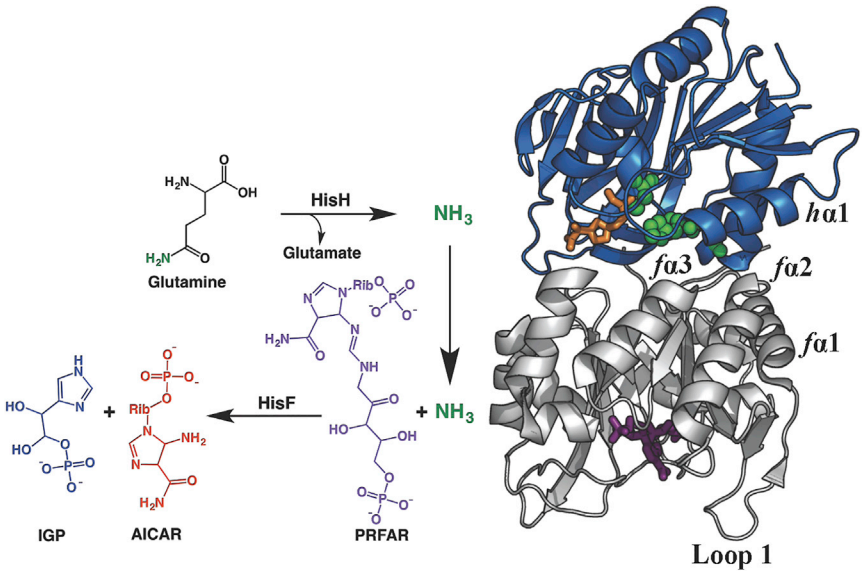

Figure 1. IGPS Reaction

The *T. maritima* IGPS complex contains two enzyme subunits: HisH (blue), which catalyzes the hydrolysis of glutamine (the Gln analog acivicin is shown in orange sticks) near a conserved catalytic triad (green spheres), and HisF (gray), which catalyzes the cleavage and cyclization of the allosteric activator and substrate PRFAR (purple sticks). The inverted arrow depicts the path of NH_3 travel, and key secondary structural elements of IGPS are labeled.

A subsequent computational analysis further demonstrated that molecular motions were involved in propagating allosteric information from the PRFAR binding site to the HisF/HisH interface (Manley et al., 2013; Rivalta et al., 2012). In particular, communication among dynamic clusters determined from network analysis is more robust when PRFAR is bound compared with the loosely connected communities of the apoenzyme. The network of dynamic residues identified in NMR and computational studies represents a putative allosteric pathway involving α helices within HisF (*f*α2, *f*α3) and HisH (*h*α1), extending from the PRFAR binding site to the dimer interface and beyond to the HisH glutaminase active site. (Throughout the text we use lowercase italicized *f* and *h* when specifically referring to residues or secondary structure elements in the HisF or HisH subunits, respectively.) Importantly, this work showed that PRFAR binding causes a merger of two separate community networks, and the location of this merger is adjacent to the bond in PRFAR that is eventually cleaved upon reaction with NH_3 (Rivalta et al., 2012). Furthermore, NMR and computational studies provided little evidence for large-amplitude ligand-induced structural changes in IGPS, instead suggesting that ligand binding activates millisecond molecular motions that enable glutaminase chemistry to occur by allowing sampling of the active conformation with the appropriate dipolar stabilization of the developing oxyanion on the glutamine substrate (Lipchock and Loria, 2010; Rivalta et al., 2012). The motions induced by PRFAR are widespread throughout the HisF subunit; however, other ligands that bind to the PRFAR site were shown to activate glutaminase activity, albeit to a lesser extent than PRFAR. This observation prompted the need to investigate whether a single allosteric network or multiple delocalized pathways are responsible for allosteric information transfer.

To further elucidate pathways in this intricate allosteric network, we examined the effects of the binding of a series of small-molecule allosteric activators on the conformational motions in IGPS. These allosteric ligands stimulate glutaminase activity in IGPS to varying degrees, with PRFAR being the most activating followed by the combination of IGP and AICAR, IGP alone, and AICAR alone(Myers et al., 2003). The enhancement of glutamine catalysis over the basal level is 4,900, 330-, 110-, and 26-fold for PRFAR, AICAR + IGP, IGP, and AICAR, respectively. Here, we detail the effects of the binding of these ligands on the structure and dynamics of IGPS. We studied binary complexes of IGPS with each of these effectors and ternary complexes that mimic the catalytic state of Gln- and PRFAR-bound IGPS by utilizing the covalently bound Gln analog, acivicin (Chittur et al., 2001). NMR analysis of the individual IGPS-ligand complexes highlights a widely dispersed and effector-dependent allosteric network in this enzyme and shows that each of these ligands is capable of stimulating millisecond motions in the HisF domain and beyond, although the number and location of these dynamic residues is variable. Interestingly, the degree to which each allosteric ligand induces conformational flexibility is intertwined with its ability to activate the enzyme.

RESULTS

Allosteric Ligand Binding Is Entropically Driven

Isothermal titration calorimetry (ITC) experiments demonstrated that PRFAR binding is an endothermic and entropically driven process (ΔH = 6.3 ± 0.04 kcal/mol and $-T\Delta S$ = −14.5 ± 0.06 kcal/mol at 298 K) (Lipchock and Loria, 2010). Endothermic ITC binding profiles for the other activating ligands, IGP and AICAR, are also observed (Figure 2). The ITC-derived K_D for IGP is 0.5 mM and is within a factor of 3 of its apparent activation constant (Myers et al., 2003). The unfavorable binding enthalpy of IGP (ΔH = 1.34 kcal/mol) is compensated by an entropic gain ($-T\Delta S$ = −5.89 kcal/mol) that drives the spontaneous process. The binding of AICAR yields reproducible isotherms with minimal enthalpy change, complicating quantitation of the integrated heat. However, previous kinetic reports (Myers et al., 2003, 2005) as well as NMR data from this work conclusively show that AICAR binds to IGPS. The K_D for AICAR obtained from NMR lineshape analysis (Figure S2) is 1.5 ± 0.2 mM, and based on this value and an estimated calorimetric $\Delta H \sim 0$, $-T\Delta S$ for AICAR binding is approximately −3.5 kcal/mol. The lineshape-derived K_D value for AICAR is similar to its apparent activation constant, K_{act} (1.3 mM) obtained from kinetic data (Myers et al., 2003). Interestingly, these ITC data show a correlation between degree of glutaminase activation by a particular allosteric ligand and the magnitude of the increase in $T\Delta S$.

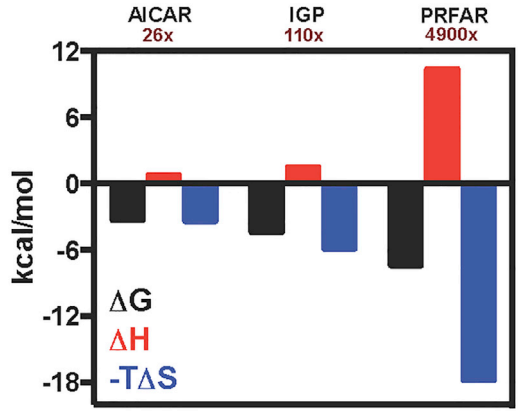

Figure 2. Ligand Binding to IGPS by ITC

Changes in free energy (black), enthalpy (red), and entropy (blue) are shown for the formation of ternary complexes through binding of AICAR, IGP, or PRFAR to acivicin-conjugated IGPS. The catalytic rate enhancements caused by each allosteric ligand are shown under the ligand label. See also Figures S1 and S2.

Allosteric Ligands Cause Small but Measurable Chemical Shift Changes

The NMR chemical shift parameter is exquisitely sensitive to the three-dimensional structure of proteins. To assess changes in the structure of IGPS caused by the formation of binary (IGPS and various effector ligands) and ternary (IGPS, effector ligand, and the covalent Gln analog, acivicin) complexes with AICAR, IGP, AICAR + IGP, and PRFAR, we monitored the chemical shifts of Ile, Leu, and Val (ILV) methyl groups as well as $^{1}H,^{15}N$ backbone amide resonances in a series of $^{1}H,^{13}C$ heteronuclear multiple-quantum coherence (HMQC) (Tugarinov and Kay, 2004; Velyvis et al., 2009) and $^{1}H,^{15}N$ transverse relaxation optimized spectroscopy (TROSY) (Pervushin et al., 1997) NMR spectra, respectively, during a titration with the ligands until IGPS was saturated. PRFAR and IGP cause the most substantial changes in HisF chemical shifts (Figure 3), yet the majority of shifts are less than 25 parts per billion. AICAR binding has an even smaller effect. Interestingly, somewhat larger chemical shift perturbations reappear when AICAR is titrated together with IGP.

Combined chemical shift differences ($\Delta\delta_{1H13C}$) reporting the magnitudes of perturbations following formation of the IGPS ternary complexes were determined from $\Delta\delta_{1H13C} = \sqrt{\Delta\delta_{1H}^2 + (0.251\Delta\delta_{13C})^2}$, where $\Delta\delta_{1H}$ and $\Delta\delta_{13C}$ are the chemical-shift differences between the effector-saturated and apo IGPS. Significant perturbations determined from the 10% trimmed mean of the $\Delta\delta_{1H13C}$ values are mapped onto the HisF structure for each ternary complex (Figure 3), highlighting regions of IGPS that are most sensitive to the presence of allosteric ligands. Several residues in close proximity to the HisF binding pocket experience the largest chemical-shift changes in the presence of these effectors. The *f*L50 methyl groups located in the HisF binding pocket and are within 3.5 Å of PRFAR appear particularly sensitive to ligand binding, as these chemical shifts are perturbed in the presence of every effector tested with the exception of AICAR (Figure S4). Furthermore, effector binding poses obtained from 100-ns molecular dynamics (MD) simulations detail the effect of HisF ligands on the *f*V48, *f*L50, and *f*l52 cluster at the *f*β2 strand, as previous results have indicated that these hydrophobic contacts are part of the IGPS allosteric pathway originating at the HisF binding pocket. Here, PRFAR binding induces disruption of the *f*L48-*f*L50 interaction, which is present in the apoenzyme, in favor of a new *f*L50-*f*l52 contact (Figure S4C), thereby altering hydrophobic interactions with the nearby loop 1 and *f*α2 helix (Rivalta et al., 2012). The MD trajectories indicate that IGP is strongly bound to IGPS via the glycerol phosphate moiety and its motion does not interfere with those of the *f*β2 hydrophobic residues (Figure S4B). AICAR, however, is also mobile at the HisF active site, weakening the *f*L50-*f*l52 contact and imposing a configuration of these residues different from that of PRFAR. This outcome is consistent with NMR data (Figure S4D) indicating that the *f*L50 resonance is not affected by the AICAR titration while it is sensitive to IGP, AICAR + IGP, and PRFAR titrations, which alter the hydrophobic *f*β2 cluster upon binding.

These small chemical-shift perturbations caused by the allosteric ligands extend beyond the HisF binding site, reaching the HisF/HisH interface in all cases. Even the weakest glutaminase activator, AICAR, perturbs ILV chemical shifts that are >15 Å away from the effector site. These data suggest the allosteric network of IGPS is widely dispersed and illuminates ligand-specific pathways that may be essential for propagation of the allosteric signal. Interestingly, IGP perturbs the chemical shifts of more residues than does PRFAR, even though it is a weaker allosteric activator, indicating that chemical-shift effects alone do not provide the entire picture of IGPS allostery (Figure 3). For example, the numbers of residues that experience significant ligand-dependent chemical shift changes are 2, 36, 23, and 15 for AICAR, IGP, AICAR + IGP, and PRFAR, respectively. Thus the two most activating allosteric ligands perturb the chemical shifts of fewer residues than lesser activating ligands. However, the allosteric pathways outlined by these chemical shift data differ with each effector, suggesting that a potential "PRFAR-specific" pathway is still the most preferable for allosteric communication.

To obtain additional insight into ligand-induced chemical shift changes, we calculated the synergistic chemical shift changes upon formation of the IGPS ternary complex. These shifts ($\Delta\Delta\delta$) were determined by comparing the chemical shift change between the apo (δ_{Apo}) and ternary ($\delta_{Ternary}$) complex versus the sum of the difference between apo and the two binary acivicin-bound ($\delta_{Acivicin}$) and effector-bound ($\delta_{Effector}$) complexes as given by $\Delta\Delta\delta = \Delta\delta_{Ternary\text{-}Apo} - (\Delta\delta_{Effector\text{-}Apo} + \Delta\delta_{Acivicin\text{-}Apo})$. Thus, values of $\Delta\Delta\delta$ that are larger than the defined cutoff value (1.5 times greater than the SD of the 10% trimmed mean value) are indicated as "synergistic" chemical shifts. This analysis shows that the PRFAR-bound IGPS enzyme undergoes a greater number (*f*V12, *f*V48, *f*L50, *f*V126, *f*L153, *f*l168, *f*L222, *f*V226, *f*V234, and *f*L237) of synergistic chemical shifts in HisF than do the other ligands (Figure S5). Analysis of $\Delta\Delta\delta$ for AICAR-bound IGPS shows only four ILV resonances with significant synergistic shifts (*f*L2, *f*V12, *f*V79, and *f*L169). The next most activating ligand, IGP, produces synergistic shifts in the resonances of eight ILV residues (*f*L2, *f*L10, *f*V12, *f*L50δ^1, *f*L50δ^2, *f*L65, *f*V126, *f*L179, *f*L222) as does the simultaneous binding of both AICAR and IGP (*f*L10, *f*l44, *f*V69, *f*V79, *f*l93, *f*V125, *f*V134, and *f*V226) shown in Figure S5. Formation of the PRFAR ternary complex

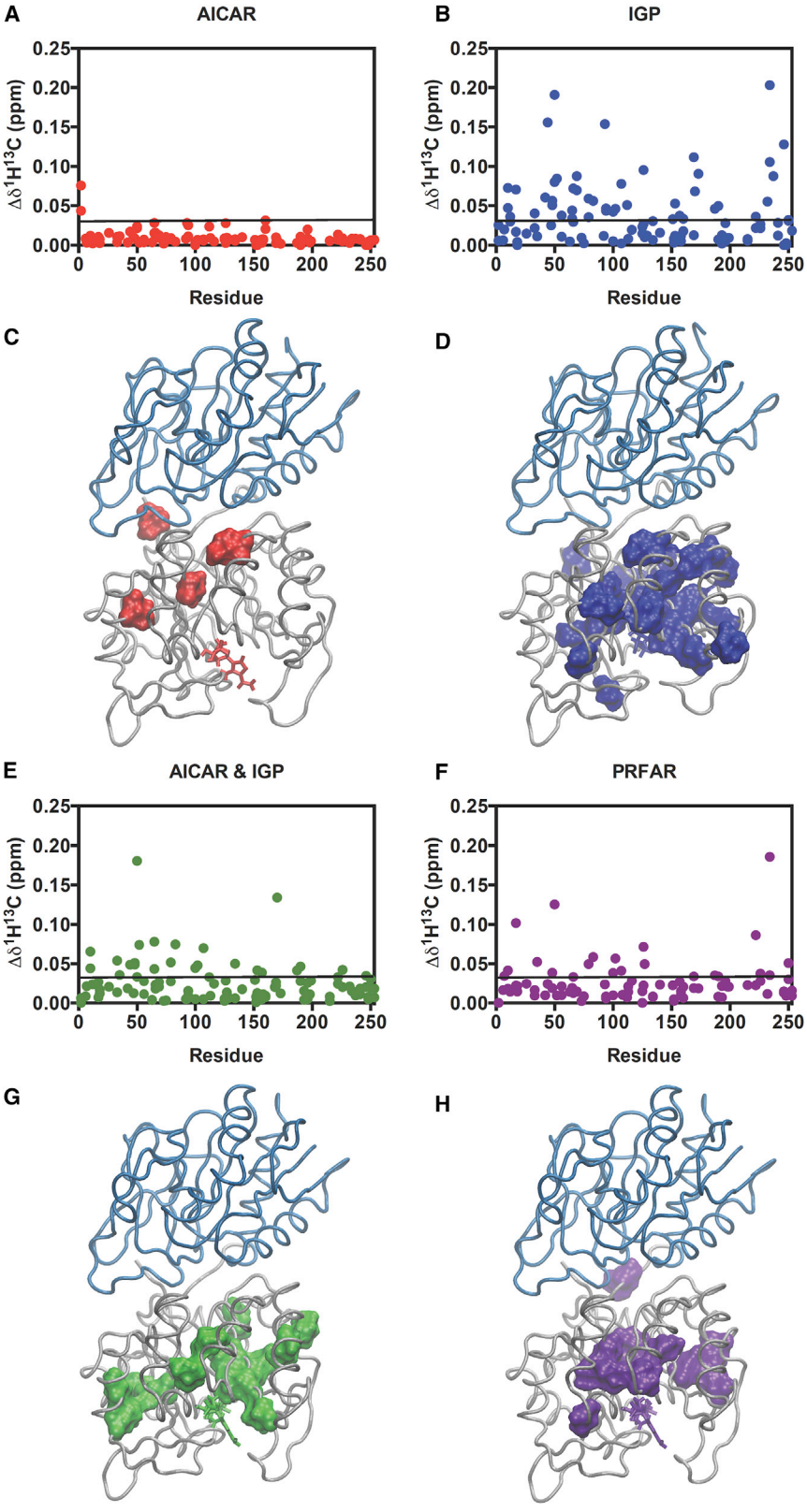

Figure 3. Ligand-Induced Chemical Shift Perturbations

(A–H) Shown are changes in (A) AICAR, (B) IGP, (E) AICAR and IGP, and (F) PRFAR effector-bound ternary complexes relative to apo IGPS. Black lines represent 1.5σ from the 10% trimmed mean of the four combined datasets. Significant changes (above the black line) are mapped onto the HisF structure (C, D, G, and H) (PDB: 1GPW) (Douangamath et al., 2002). See also Figures S3–S5.

induces synergistic perturbations in ten ILV residues, only half of which show significant ΔΔδ in the analysis of other effectors. Thus, synergistic changes in the chemical shifts of *f*V48, *f*L153, *f*I168, *f*V234, and *f*L237 are exclusive to PRFAR-bound IGPS, suggesting they or residues nearby may be particularly important for allostery in the formation of the most enzymatically active complex. In support of this, mutagenesis of residues *f*D98, *f*K99, *h*Y138, and *h*K181, which are adjacent to these residues, cause a varying degree of allosteric defects in IGPS, presumably through disruption of the interfacial salt bridges proposed to regulate NH_3 transport to HisF (List et al., 2012). Furthermore, the significant number of ligand-dependent differences in this synergy, especially those found in comparison with the PRFAR-bound ternary complex, indicates there are likely multiple allosteric networks within IGPS. Thus, the best allosteric activator does not cause large chemical-shift changes in the majority of residues in comparison with other ligands, but PRFAR binding does result in the largest number of residues with synergistic chemical shift changes. Moreover, the number of synergistic chemical shift changes correlates well with the activating power to the allosteric ligands.

The Allosteric Signal Travels to the HisH Active Site

The allosteric signal resulting from ligand binding in HisF must travel more than 25 Å to the glutaminase active site of HisH. Previous work suggested that PRFAR, rather than causing large-amplitude structural changes, induces millisecond motions that result in temporal sampling of the catalytically active HisH structure without large deviations from the most populated, inactive solution structure. It is possible that sampling of the active conformer occurs more readily when PRFAR is bound compared with the other allosteric effectors. Crystallographic (Chaudhuri et al., 2001, 2003; Douangamath et al., 2002), NMR (Lipchock and Loria, 2010), and MD (Manley et al., 2013; Rivalta et al., 2012)

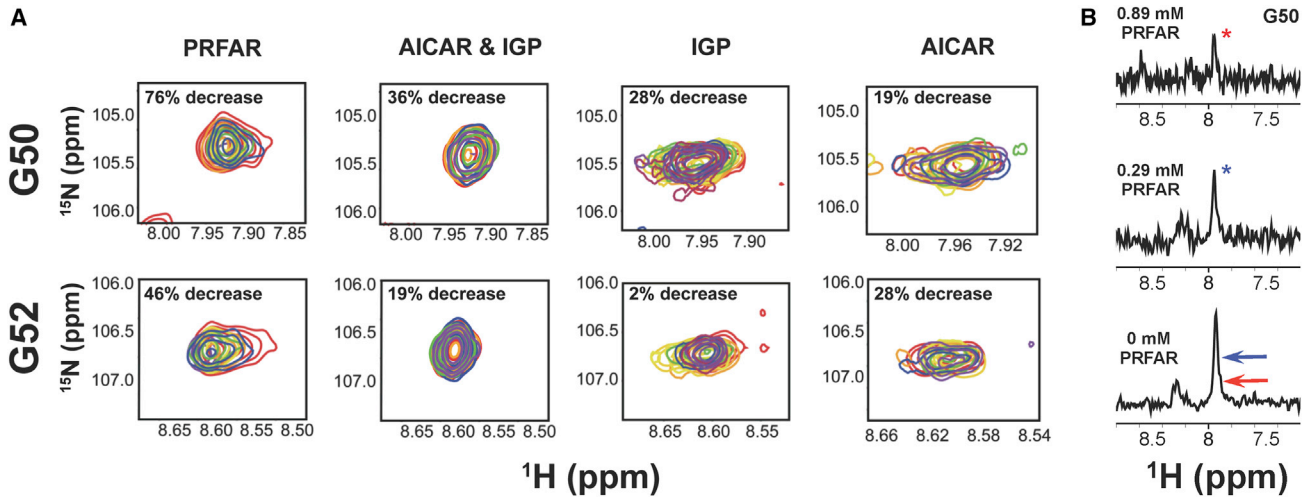

Figure 4. Ligand-Induced Exchange Broadening of *h*G50 and *h*G52 Located in the HisH PGVG Loop

(A) The ligand titration ranges from red (apo) to purple (effector-saturated), and the percentage decrease in peak intensity is shown.

(B) One-dimensional slices of the *h*G50 resonance showing the decrease in peak intensity from PRFAR binding. Relative peaks heights of the ligand-bound resonances (red and blue asterisks) are shown by arrows in the bottom panel.

studies suggest that a rotation of the HisH active site *h*Pro49-*h*Gly50-*h*Val51-*h*Gly52 (PGVG) loop, which lies adjacent to the HisH catalytic triad, is required for proper formation of the oxyanion hole during catalysis, although double-mutant studies suggest additional factors are essential for HisH catalysis (List et al., 2012). To examine long-range perturbations at the glutaminase site caused by effector binding, we monitored the amide backbone chemical shifts of the *h*G50 and *h*G52 resonances of the PGVG loop during allosteric ligand titration into ^{2}H,^{15}N-labeled HisH-IGPS (Figure 4).

Similar to our observations in HisF, we detected very small chemical shift changes in the *h*G50 and *h*G52 resonances during titration with PRFAR and no changes during titration with IGP or AICAR. However, a significant amount of exchange broadening is observed (Figure 4), indicative of enhanced millisecond motions at these residues. These ligand-induced motions at the HisH active site are consistent with MD simulations that showed greater flexibility in the PGVG loop residues in the presence of PRFAR (Manley et al., 2013; Rivalta et al., 2012). The extent of the broadening is effector dependent for *h*G50 and *h*G52, where saturation with PRFAR results in a 76% and 46% decrease in peak intensity, respectively, relative to that in apo IGPS. The combination of AICAR and IGP has a greater effect than either ligand alone, most notably on *h*G50, which is broadened by 36%. IGP broadens *h*G50 by 28%, but has a minimal effect on *h*G52. AICAR binding decreases the intensities of the *h*G50 and *h*G52 resonances by 19% and 28%, respectively. Interestingly, the degree of exchange broadening found in these HisH PGVG loop residues correlates with effector strength, especially for *h*G50. More importantly, these data demonstrate that all allosteric ligands can induce motional changes that span the dimer interface, reaching the HisH active site. Thus, these data indicate that PRFAR alters the motions at the HisH active site more significantly than all other activators, and the degree to which motions are altered is loosely correlated with the effectiveness of allosteric activation.

Allosteric Ligands Induce Millisecond Motions in HisF

Formation of IGPS ternary complexes results in ligand-induced exchange broadening of HisF resonances in the ^{1}H,^{15}N TROSY heteronuclear single-quantum coherence (HSQC) spectra of each effector-bound IGPS complex (Figure 5). Binding of AICAR to a preformed complex of acivicin-IGPS causes broadening of four amide resonances, although two of these, *f*L10 and *f*L253, lie at the PRFAR binding site and the HisF/HisH interface, respectively (Figure 5B). Ternary complexes containing IGP and AICAR + IGP show similar but amplified effects on the HSQC spectrum of HisF-IGPS, as 32 and 34 resonances, respectively, are broadened beyond detection (Figures 5C and 5D). Both effectors induce broadening near the ligand site as well as the dimer interface. Additional broadening is observed in loop 1, adjacent to the effector binding site, and the *f*α1 and *f*α3 helices. The combination of AICAR and IGP also broadens small clusters of resonances belonging to *f*α2, *f*α4, and *f*α6. Most strikingly, PRFAR binding causes 65 (25% of HisF) residues to be broadened beyond detection (Figure 5A). Clusters of broadened resonances in the PRFAR complex correspond to amino acids near the ligand binding site, loop 1, the dimer interface, and smaller subsets of resonances from *f*α1 to *f*α7 (Figures 5A and 5E).

A lesser degree of exchange broadening was observed in the ^{1}H,^{13}C TROSY HMQC spectra monitoring ILV residues of each effector-bound IGPS complex, allowing additional investigation into these effects using NMR relaxation methods. To better quantitate ligand-induced millisecond motions, we compared ILV-based NMR CPMG (Carr-Purcell-Meiboom-Gill) relaxation dispersion experiments on binary and ternary complexes of AICAR-, IGP-, AICAR + IGP-, and PRFAR-bound HisF-IGPS.

Millisecond Motions Occur in All Effector-Bound Complexes

A comparison of the millisecond motions in binary and ternary IGPS complexes show a number of similarities. Here, focus is

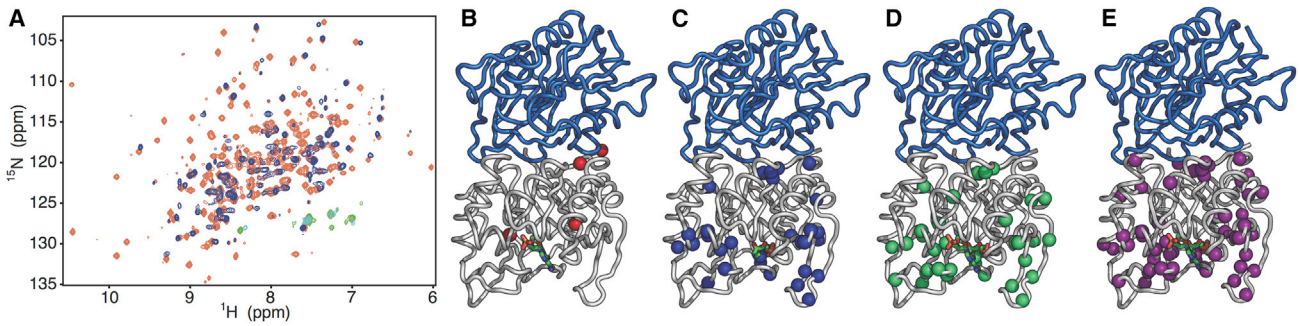

Figure 5. Ligand-Induced Exchange Broadening in HisF

(A–E) Representative ^{1}H,^{15}N HSQC spectrum of apo IGPS (orange) and PRFAR-bound IGPS (purple) (A). Residues that are significantly broadened in the presence of allosteric effectors are mapped onto the IGPS structure for AICAR (B), IGP (C), AICAR and IGP (D), and PRFAR (E) complexes. See also Figure S3.

restricted to the differences among the ternary complexes given their particular relevance to the active form of an allosteric enzyme (Kimmel and Reinhart, 2000). A summary of the NMR results for all binary and ternary complexes is provided in Tables S1–S6.

Formation of each ternary complex results in changes in the millisecond motions at numerous amino acid sites. Figure 6 shows distinct CPMG relaxation dispersion profiles caused by the different allosteric activators for residues located throughout IGPS. Non-linear fitting of the dispersion curves results in unique rate constants (k_{ex}) for motion of each residue, with the PRFAR-bound ternary complex being the exception where the motion of all residues are better represented with a single k_{ex} value of 225 ± 30 s^{-1}.

Formation of the ternary PRFAR complex induces millisecond motion in 36 ILV methyl groups, eight of which are unique to this ternary complex: *f*V12, *f*V17, *f*V48, *f*L63, *f*I116, *f*V140, *f*V190, and *f*L196. As noted above, all 36 methyl groups in the PRFAR ternary complex are well described by a single k_{ex} value, suggesting concerted motions in this most catalytically active ternary complex. All other binary and ternary complexes exhibit millisecond motions with large ranges of k_{ex} values (Figures 6 and 7). A number of the motions detected in the PRFAR ternary complex result from the presence of both acivicin and PRFAR, and these motions are not detected in their respective binary complexes.

Similarly, millisecond motions occur for a unique subset of residues in IGPS ternary complexes containing AICAR, IGP, and AICAR + IGP when compared with their corresponding binary state (Tables S1–S7). In the ternary complex fewer ILV methyl groups undergo conformational exchange in AICAR, IGP, and AICAR + IGP enzyme forms compared with those in the PRFAR complex. However, these motions remain interspersed throughout the HisF $\alpha_8\beta_8$ barrel (Figure 8). PRFAR-induced motions are widespread in IGPS, whereas dynamic residues within the other ternary complexes are primarily located in the β strands of the HisF barrel. No millisecond motions were detected for residues in the HisF helices α4, α5, α6, or α7 surrounding the β barrel in the IGP and AICAR + IGP complexes, unlike those observed for PRFAR. Thus, the left side of the HisF subunit (as oriented in Figure 8), in which the ribonucleotide portion of PRFAR binds, appears more static in ternary complexes with weaker effectors. A lack of flexibility in this region of HisF becomes more evident in the AICAR ternary complex, where even fewer secondary structural elements contain dynamic ILV residues. Millisecond motions are absent from the α1, α4, α5, α6, α7, and α8 helices and the β4, β5, β6, and β7 strands, confining the 18 dynamic methyl groups to a small region of HisF when AICAR is bound. Interestingly, there is a linear correlation between the number of flexible residues induced by a particular ligand and the enhancement of k_{cat}/K_M for glutaminase activity (Figure 8A).

Unique motions in the PRFAR ternary complex extend from the HisF ligand site to the HisF/HisH interface and are dispersed throughout the domain (Figure 8). The locations of uniquely flexible residues in the ternary complex containing AICAR and IGP are similar to those found with PRFAR, occurring near the HisF active site and dimer interface. However, flexible residues unique to the IGP- and AICAR-bound ternary complexes are concentrated exclusively near the HisF/HisH interface. Differences in the number and identity of flexible residues among the ternary complexes points to an allosteric network with multiple pathways of information relay between the cyclase and glutaminase active sites.

The concerted motions observed in the PRFAR ternary complex are not observed for any other allosteric ligand. Relaxation dispersion profiles measured for IGPS ternary complexes containing AICAR, IGP, and AICAR + IGP cannot be described by a single global process, and non-linear fits of these dispersion data yield a range of k_{ex} values, many of which are significantly higher than the exchange-rate constant determined for the PRFAR complex. The fastest rates of conformational exchange are found in the IGP complex, with values of k_{ex} ranging from ~1,000 to 6,000 s^{-1}. Exchange rates measured for ILV methyl groups in the AICAR + IGP-bound ternary complex are in a slower regime, but some still have a maximum k_{ex} value of 4,900 s^{-1}. Conformational exchange is slowest in the AICAR ternary complex, occurring at a rate nearly identical to that of its corresponding binary complex (200–1,500 s^{-1}) with the exception of a single residue, *f*I44. These ligand-induced motions are due to conformational exchange in IGPS and not from binding and dissociation of the ligands themselves. Values of k_{on} and k_{off} for each ligand obtained by NMR lineshape analysis indicate that the rates of ligand binding and unbinding are too fast to contribute to the CPMG dispersion data. Thus, these data reflect motions within the enzyme itself.

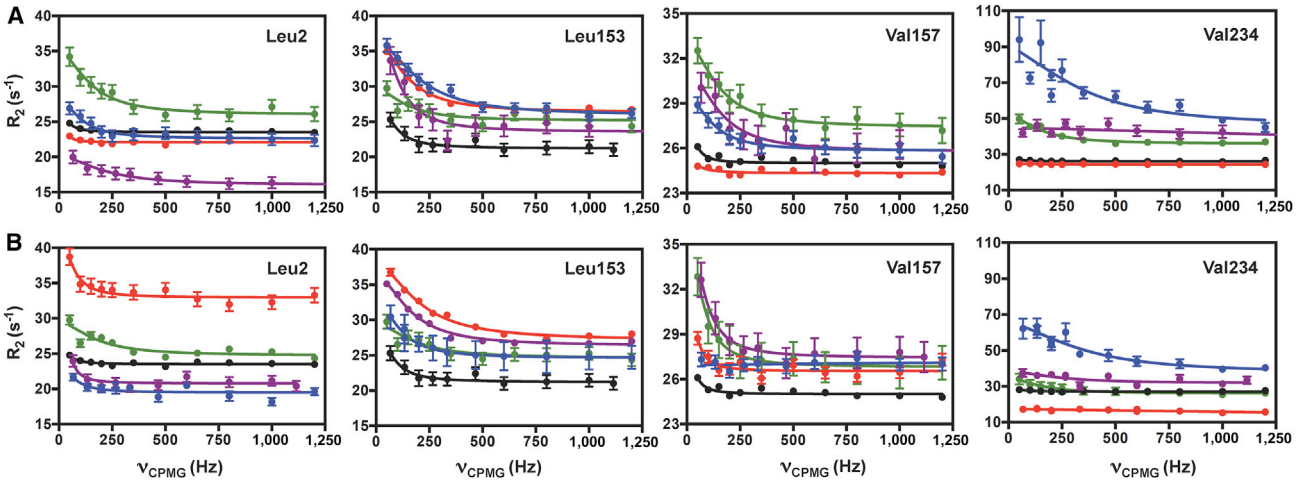

Figure 6. Ligand-Induced Millisecond Motions in IGPS

(A and B) Representative CPMG curves for (A) effector-bound binary and (B) ternary complexes of IGPS for apo (black), AICAR (red), IGP (blue), AICAR and IGP (green), and PRFAR (purple) IGPS. Error bars were determined from duplicate experiments. See also Table S1 and Figure S8.

The individually determined k_{ex} values mapped onto the structures of AICAR-, IGP-, and AICAR + IGP-bound IGPS reveal local clusters of similar exchange rates in all complexes. With the exception of the IGP ternary complex (Figure 7), most flexible residues experience motions slower than 1,500 s^{-1} (Figure S6). Smaller clusters of residues undergoing faster motions generally occur near the effector binding site and along the α helices of the HisF barrel. These clusters, regardless of effector ligand and motional regime, universally form connective pathways from the HisF binding site to the dimer interface, which in some cases involve multiple routes. However, differences in the kinetic regimes of dynamic clusters could hinder efficient transfer of allosteric information.

Interestingly, nearly every flexible residue in the IGP ternary complex is shifted to a higher exchange timescale than that of the analogous PRFAR complex (Figure 7). Thus, the rate of conformational exchange is also not the sole determinant of activator efficiency, suggesting that a delicate balance exists between the number, location, and timescale of motions in HisF.

The ability to stimulate concerted conformational fluctuations appears to be unique to PRFAR, suggesting that non-concerted motions or motions faster than ~230 s^{-1} are less than optimal for catalytic activation and may partially explain the weakened activating power of IGP and AICAR. Although AICAR and IGP are allosteric activators of IGPS, there are significant gaps in the abilities of these effectors to enhance glutamine hydrolysis (4,900-fold increase with PRFAR, 110-fold for IGP, and 26-fold for AICAR). The differences between the conformational exchange rates measured for the PRFAR-bound ternary complex and those containing AICAR, IGP, or AICAR + IGP suggest that enhancement of millisecond motions alone are not enough to effectively relay allosteric information to the HisH active site. It appears that controlled, concerted motion in specific *locations* throughout the HisF domain provides the proper conformational fluctuations that are essential for efficient glutaminase activation, which is unique to the PRFAR-bound ternary complex.

DISCUSSION

The enhancement of millisecond motions in IGPS is vital to communication between the HisF and HisH active sites. Numerous experimental studies of IGPS demonstrate a lack of structural change upon effector binding (Chaudhuri et al., 2001, 2003; Douangamath et al., 2002; Lipchock and Loria, 2009, 2010; List et al., 2012; Rivalta et al., 2012; Vanwart et al., 2012), ruling out significant conformational changes as a means of relaying allosteric information. The X-ray crystal structures of apo and PRFAR-bound IGPS (PDB: 1OX4 and 1OX5, respectively) reveal negligible changes in the structure due to PRFAR binding (root-mean-square deviation = 0.41 Å) (Chaudhuri et al., 2003). Furthermore, fluorescence quenching experiments examining solvent accessibility at the HisF/HisH interface yield the same results for apo, acivicin, binary PRFAR-bound, and ternary PRFAR-bound complexes, suggesting minimal differences in these structures (Lipchock and Loria, 2010). However, a striking difference between apo IGPS and the allosterically activated enzymes is the ligand-enhanced millisecond motions. The extent of line broadening in the $^{1}H,^{15}N$ HSQC NMR spectrum of HisF-labeled IGPS during titrations with PRFAR indicate that this ligand causes a change in backbone amide motion on the millisecond timescale, with more than 25% of the amide resonances being broadened beyond detection. NMR relaxation experiments additionally demonstrate enhancement of conformational fluctuations in the $^{13}CH_3$ groups of ILV residues within IGPS, when bound to PRFAR (Lipchock and Loria, 2010).

To more fully understand the role of conformational fluctuations in IGPS allosteric signaling, we investigated the interactions of additional allosteric effectors, AICAR, IGP, and AICAR + IGP, with IGPS. These effectors provide a scale of chemical probes that are known to activate the glutaminase domain to different extents. Motions of the methyl groups of ILV residues within HisF were quantified in both binary and ternary complexes with AICAR, IGP, and AICAR + IGP with CPMG relaxation dispersion experiments. Based on these data, we have established a

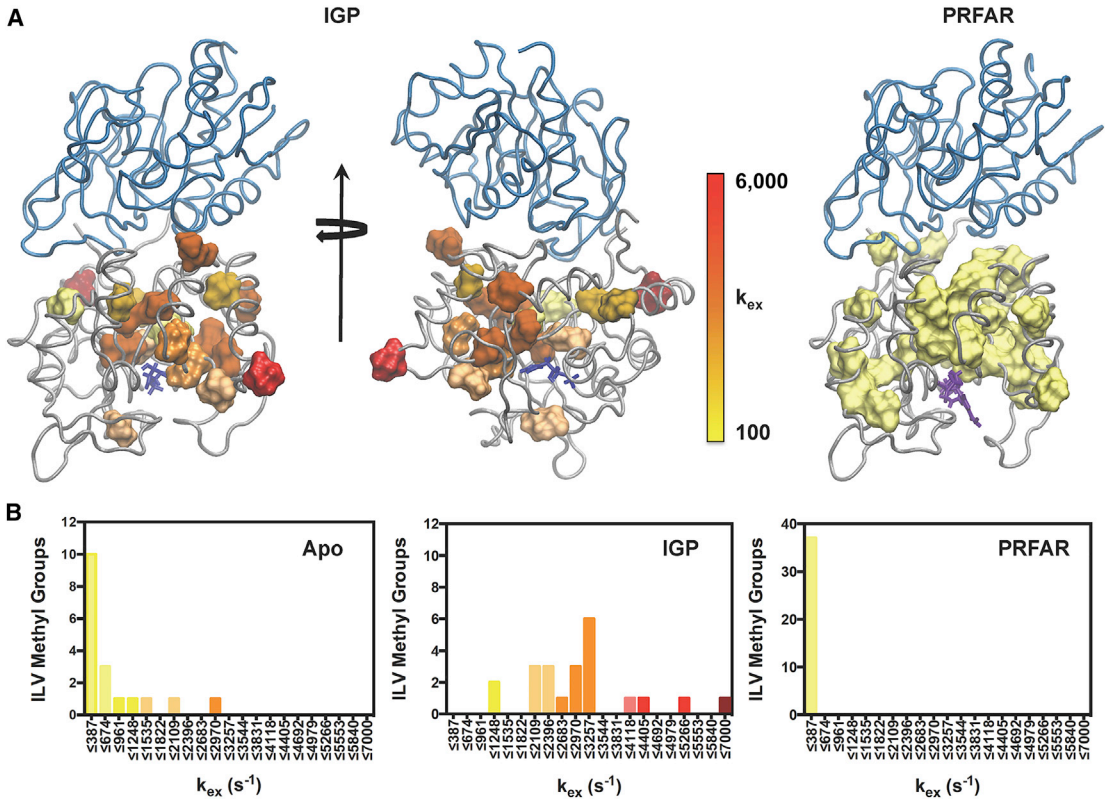

Figure 7. Structural Clustering of k_{ex} from NMR Relaxation Dispersion

(A) The magnitudes of k_{ex} are mapped onto the structure of the IGP (left and middle) and PRFAR (right) ternary complexes for all residues undergoing millisecond exchange. Other IGPS complexes are in Figure S7.

(B) Distribution of k_{ex} values for the apoenzyme (left), IGP ternary complex (middle), and PRFAR ternary complex (right). Colors in each histogram correlate with (A). Optimal bin sizing for these data were determined using the protocol outlined in Scott (1979). IGP and PRFAR are represented by blue and purple sticks, respectively. See also Tables S2–S7 and Figure S6.

relationship between the glutaminase activation potential of allosteric ligands and the number of residues experiencing millisecond conformational flexibility. The increase in conformational flexibility caused by allosteric ligands also correlates with ITC measurements, which showed a trend in enthalpy/entropy compensation of AICAR, IGP, and PRFAR binding in which the more activating ligand is more enthalpically disfavored and more entropically favored (Figure 2).

Comparison of millisecond motions in AICAR-, IGP-, AICAR + IGP-, and PRFAR-bound ternary complexes reveals that better glutaminase activators cause a larger number of amide and ILV methyl groups to undergo millisecond conformational exchange (Figure 8). The location of these dynamic residues is also important as PRFAR, the native allosteric ligand, imparts the greatest degree of flexibility to the α helices and β strands of the $\alpha_8\beta_8$ barrel at the center of HisF. AICAR + IGP and IGP alone are significantly weaker allosteric activators and, although motions present in each of these ternary complexes are also spread around the HisF $\alpha_8\beta_8$ barrel, they occur primarily on the β strands. The weakest allosteric activator, AICAR, is capable of enhancing flexibility of only one-half of the $\alpha_8\beta_8$ barrel, reminiscent of motions observed in apo and acivicin-bound IGPS. Millisecond motions are enhanced in β1, α2, β2, β3, and β8 of every ternary complex (Figure 8), suggesting that these regions of HisF are fundamental to relaying allosteric information. However, optimal allosteric signaling requires domain-wide flexibility that includes additional structural elements within the $\alpha_8\beta_8$ barrel, namely in the α helices. Flexibility around the entire HisF barrel is presumably necessary for the highest level of glutaminase activation because it promotes fluctuations in the distances of the charged gate residues (*f*R5, *f*E46, *f*K99, and *f*E167), which are proposed to regulate the passage of NH_3 across the interface.

A number of biochemical studies have identified amino acids that are critical for relaying allosteric information between the PRFAR binding site and the glutaminase site in HisH (Amaro et al., 2007; Beismann-Driemeyer and Sterner, 2001; Chaudhuri et al., 2003; Chittur et al., 2001; Klem and Davisson, 1993). Many of those residues also show millisecond motions in the IGPS complexes studied here. Four residues make up the salt bridge gate noted above. Of those, the amides of *f*K99 and *f*E167 are not assigned but adjacent residues *f*D98, *f*G96, *f*V100, and *f*V102 are assigned, as are *f*L169 and *f*L170. PRFAR stimulates millisecond motions for all of those gate residues or residues adjacent to the gate (*f*A3, *f*I6, *f*V48, *f*G96, *f*D98, *f*V100, *f*V102, *f*L169, and *f*L170). AICAR + IGP, IGP, and AICAR only activate millisecond motions in a subset of these residues. Notably, residues near *f*K99 are only flexible when PRFAR is bound.

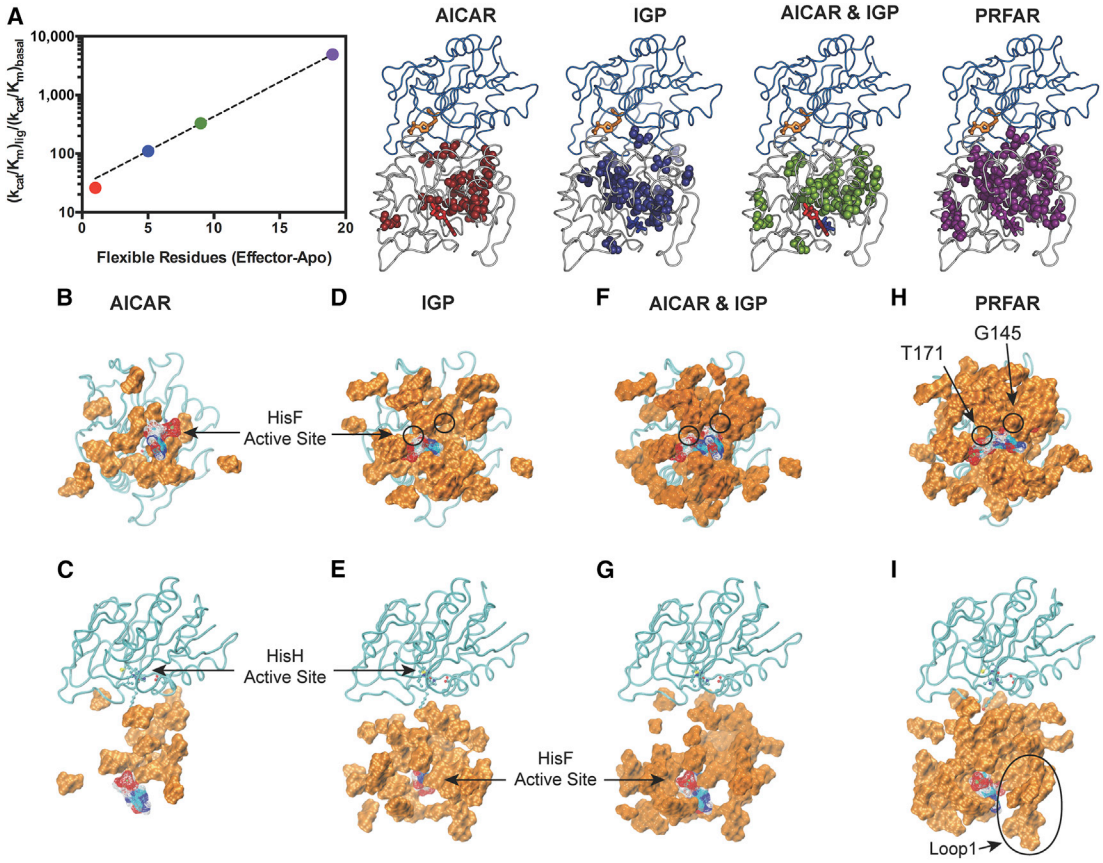

Figure 8. Flexible Residues and Catalytic Rate Enhancement in IGPS

(A) Correlation of k_{cat}/K_M versus the number of ILV residues that experience millisecond motions as determined from CPMG relaxation dispersion measurements for AICAR, IGP, AICAR and IGP, and PRFAR ternary complexes.

(B–J) Flexible residues that show ligand-induced ILV dispersion curves or amide exchange broadened (beyond detection) in each of the ternary complexes. (C, E, G, and I) Rotated views of (B), (D), (F), and (H), respectively. Residues are shown as a surface rendering with each active site labeled. The allosteric ligands are shown as wire mesh. The HisH subunit is shown in cyan.

See also Figures S7 and S8.

Mutation of loop-1 residue *f*K19 results in reduced allosteric communication in IGPS. *f*K19 is a critical component of the flexible region of loop 1 that may interact with allosteric ligands in the cyclization site, consistent with a significant increase in the normal 1:1 stoichiometry of glutamine hydrolysis/PRFAR cleavage in *f*K19 mutants (Beismann-Driemeyer and Sterner, 2001). The ^{1}H,^{15}N amide of *f*K19 is not assigned. Nonetheless, binding of PRFAR results in enhanced motions in *f*T21, *f*G20, *f*V18, *f*V17, and *f*V12 all located in loop 1. The other ligands again only enhance millisecond motions in a subset of these residues. Thus, these ligands result in enhanced flexibility in amino acid residues that are known to be critically important for allostery.

The β strands in IGPS are more conserved than the α helices (Figure S8). The two weaker allosteric ligands, AICAR and IGP, primarily enhance motions in the conserved β strands of the $\alpha_8\beta_8$ barrel, while PRFAR and, to a lesser extent, AICAR + IGP induce conformational flexibility throughout all secondary structural elements of HisF. Thus, ligand-induced motions within the highly conserved β strands of HisF may be an intrinsic property of IGPS, regardless of effector, while additional flexibility in the α helices of the HisF barrel more strongly influences the ability of allosteric ligands to activate *T. maritima* IGPS.

The extent of motions in a number of β strands and several other localized regions of HisF in response to AICAR, IGP, AICAR + IGP, and PRFAR binding indicates that the allosteric network of IGPS is disperse. These data are consistent with several investigations of IGPS mutants, which have primarily concentrated on the HisF binding pocket and the HisF/HisH interface. Smaller numbers of mutants affecting the HisF $\alpha_8\beta_8$ barrel were reported to disrupt glutaminase activity (Beismann-Driemeyer and Sterner, 2001; List et al., 2012). Our NMR chemical shift titrations and CPMG relaxation dispersion measurements indicate that numerous residues along the $\alpha_8\beta_8$ barrel, such as *f*Leu50, *f*Val126, and *f*Leu222 undergo significant changes in chemical shifts and millisecond dynamics, lending support to the importance of mutational studies in the barrel region of HisF (Figures S4 and S5).

In addition to the effects of allosteric ligands on the HisF domain of IGPS, NMR line broadening also indicates millisecond motional changes in the HisH PGVG loop during chemical shift titrations, consistent with a dynamic mechanism involving loop

rearrangement to the catalytically competent form of the enzyme (Rivalta et al., 2012). The ability of allosteric effectors to induce broadening provides evidence that binding information in HisF is relayed across the dimer interface.

The obvious difference between PRFAR and the lesser activating ligands is the chemical linkage at the C7 position joining the AICAR portion to the uncyclized glycerol phosphate moiety. Interestingly, the site of bond cleavage and cyclization near C7 is positioned next to two HisF residues (G145 and T171) that only demonstrate flexibility when PRFAR is bound. The backbone amide of *f*G145 interacts with PRFAR through a bound water molecule, and the hydroxyl side chain of *f*T171 is within H-bonding distance of N8 and the 2″ carbonyl of PRFAR. Simultaneous binding of AICAR and IGP only increases the flexibility of G145, whereas only T171 is flexible when IGP binds. Thus it is possible that these two residues "sense" the presence of PRFAR and are the initiators of the concerted millisecond motions only observed in this complex.

The NMR data in this work are not consistent with a two-site population shift between inactive (apo) IGPS and an active structure. If this were the case it would be expected that the ligand-induced shifts would follow a linear trend, with PRFAR causing the largest shifts with the magnitude of other ligand-induced shifts being commensurate with their activating power. This is not what is observed (Figure S5). In some cases the shifts are linear and PRFAR does cause the largest change, but in the majority of cases the largest chemical-shift perturbation is caused by IGP binding (Figure S5). In addition, for a number of residues there is no linear trend among the ligands. Although the data are consistent with a ligand-induced effect, it does not support a two-state T-to-R-like transition between distinct structures.

The R_{ex} parameter ($R_{ex} = p_a p_b \Delta\omega_H \Delta\omega_C$) determined from relaxation dispersion experiments contains useful structural information about the lowly populated conformer in solution (Beach et al., 2005; Grey et al., 2003; Massi et al., 2006). Previous studies (Beach et al., 2005; Boehr et al., 2006) have noted a correlation between R_{ex} and $\Delta\omega$ that provides supportive evidence for the so-called conformational selection model. In this work, we observe no correlation between the ligand-induced chemical shift changes and R_{ex} (Table S7). Moreover, the magnitude of R_{ex} is not correlated with the activating power of the ligands. For example, on a per-residue basis, R_{ex} for the IGP ligand is greater than that for PRFAR. These data seem to support a broadening of the ensemble of enzyme conformations while the average solution conformation does not change significantly. Within this ensemble it seems likely that multiple active states exist, and PRFAR allows for more efficient sampling of these active conformations.

In conclusion, we have used several small-molecule effectors with varying abilities to activate the IGPS glutaminase domain to gain insight into the allosteric mechanism of this enzyme, specifically, the role that millisecond motions play in allosteric communication between the HisF and HisH active sites. Enhancement of millisecond motions in the highly conserved β1, β2, β3, and β8 strands of HisF are fundamental for allosteric signal transmission, but flexibility around the entire $\alpha_8\beta_8$ barrel appears necessary for the most efficient glutaminase activation. Conformational fluctuations around the HisF barrel hint at an allosteric mechanism that relies on "unplugging" the gated path at the HisF/HisH interface, allowing transportation of NH_3 between domains. We also find that the number of ILV methyl groups undergoing conformational exchange in binary and ternary effector-bound IGPS complexes correlates with the activating power of the ligand. This conformational exchange is a concerted motional process in PRFAR-bound IGPS; however, residues in ternary complexes containing AICAR, IGP, and AICAR + IGP undergo asynchronous motions that generally occur much more quickly (>1,000 s^{-1}). Thus, the concerted motion measured in the PRFAR-bound ternary complex sets it apart from other effectors and may contribute significantly to its high activating power. The results presented in this work reveal an intricate balance of contributions from the number, location, and rate of motions within HisF and outline important differences among these complexes that provide insight into the allosteric mechanism of IGPS.

EXPERIMENTAL PROCEDURES

Materials

AICAR and the glutamine analog acivicin were purchased from Sigma. IGP (D-erythroimidazole glycerol phosphate) was purchased from Santa Cruz Biotechnology. Antibiotics used in protein expression and other analytical-grade chemicals were purchased from AmericanBio. PRFAR was synthesized as previously described (Lipchock and Loria, 2010).

Acivicin Labeling

Covalent modification of IGPS with the non-hydrolyzable Gln analog acivicin was achieved by incubating IGPS with two molar equivalents of acivicin for 8–10 hr (Chittur et al., 2001; Lipchock and Loria, 2010). A reduction in free thiol (Cys) content was confirmed with a DTNB (5,5′-dithio-bis-(2-nitrobenzoic acid)) assay. Excess acivicin was removed by dialysis against 10 mM HEPES (with 10 mM KCl and 0.5 mM EDTA) buffer at pH 7.3, and IGPS was subsequently concentrated using an Amicon centrifugal cell.

Isothermal Titration Calorimetry

ITC measurements were carried out using a MicroCal iTC 200 using 19 × 2.0-μl injections of ligand after an initial 0.2-μl injection, with 250-s spacing between injections. IGPS was prepared by dialysis against 2 × 4.0 l of 50 mM HEPES (pH 7.6) with 10 mM KCl. Final IGPS concentration was measured by UV absorbance at 280 nm (ε = 29,005 M^{-1} cm^{-1}). Experimental concentrations of IGPS were 0.15 mM (stoichiometrically modified with acivicin) while effector concentrations were 1.14, 13, and 20 mM for PRFAR, IGP, and AICAR, respectively.

NMR Titrations

NMR titrations were performed on a 14.1-T Varian Inova NMR spectrometer at 30°C by collecting a series of ^{1}H,^{13}C TROSY HMQC and ^{1}H,^{15}N TROSY HSQC spectra with increasing ligand concentration. The ^{1}H and ^{13}C carrier frequencies were centered at 0.75 and 19.5 in the HMQC while the ^{1}H and ^{15}N carrier frequencies were set to the water resonance and 120 ppm, respectively. Saturation of HisF-IGPS was monitored by following resonance shifts until additions of ligand produced no further perturbation. PRFAR was titrated to a concentration of 0.9 mM, IGP to a concentration of 12 mM, and AICAR to a concentration of 14 mM. The NMR-observed ligand saturation point is consistent with the expected values based on prior ITC experiments.

Methyl-TROSY Multiple-Quantum CPMG Dispersion Experiments

Multiple-quantum CPMG experiments probing ILV methyl groups ($^{13}CH_3$) were performed on 14.1-T Varian Inova and 18.8-T Agilent NMR spectrometers at 30°C. The methyl-TROSY CPMG pulse sequence was based on the report of Kay and coworkers (Korzhnev et al., 2004a, 2004b). A constant relaxation delay period of 40 ms was used in the CPMG sequence, with varied τ_{cp} points of 0.0, 0.4167, 0.50, 0.625, 0.7682, 1.0, 1.4286, 2.0, 2.5, 3.333, 5.0, and 10.0 ms, with a recycle delay of 2.0 s.

Data Analysis and Processing

NMR spectra were processed with NMRPipe (Delaglio et al., 1995) and analyzed in SPARKY (Goddard and Kneller, 2008). Transverse relaxation rates (R_2) were determined by measuring peak intensities of each ILV methyl resonance at multiple τ_{cp} delay points with a Perl-based exponential curve-fitting script. Relaxation dispersion curves were generated by plotting R_2 versus $1/\tau_{cp}$ using RELAX (Bieri et al., 2011; d'Auvergne and Gooley, 2008a, 2008b) with the R_{2eff}, NoR_{ex}, and MMQCR72 (full two-site Carver-Richards) models (Morin et al., 2014). Relaxation dispersion data obtained at two static magnetic fields were fit simultaneously using the fast CPMG equation and uncertainty values were obtained within RELAX from replicate spectra.

SUPPLEMENTAL INFORMATION

Supplemental Information includes Supplemental Experimental Procedures, eight figures, and seven tables and can be found with this article online at http://dx.doi.org/10.1016/j.str.2016.04.010.

AUTHOR CONTRIBUTIONS

J.P.L. and V.S.B. designed the research; G.P.L. and G.A.M. performed the research; G.P.L., G.A.M., and J.P.L. analyzed the data; G.P.L. and J.P.L. wrote the paper; I.R. and V.S.B. designed computational research; H.H. and I.R. performed computational work; I.R. and V.S.B. wrote computational work.

ACKNOWLEDGMENTS

This work was supported by NIH grant GM106121 to J.P.L. and V.S.B. We thank Kyle East for assistance with lineshape analysis.

Received: March 11, 2016
Revised: April 20, 2016
Accepted: April 22, 2016
Published: May 26, 2016

REFERENCES

Amaro, R.E., Sethi, A., Myers, R.S., Davisson, V.J., and Luthey-Schulten, Z.A. (2007). A network of conserved interactions regulates the allosteric signal in a glutamine amidotransferase. Biochemistry *46*, 2156–2173.

Bahar, I., Chennubhotla, C., and Tobi, D. (2007). Intrinsic dynamics of enzymes in the unbound state and relation to allosteric regulation. Curr. Opin. Struct. Biol. *117*, 633–640.

Bakan, A., and Bahar, I. (2009). The intrinsic dynamics of enzymes plays a dominant role in determining the structural changes induced upon inhibitor binding. Proc. Natl. Acad. Sci. USA *106*, 14349–14354.

Beach, H., Cole, R., Gill, M., and Loria, J.P. (2005). Conservation of μs-ms enzyme motions in the apo- and substrate-mimicked state. J. Am. Chem. Soc. *127*, 9167–9176.

Beismann-Driemeyer, S., and Sterner, R. (2001). Imidazole glycerol phosphate synthase from *Thermatoga maritima*: quaternary structure, steady-state kinetics, and reaction mechanism of the bienzyme complex. J. Biol. Chem. *276*, 20387–20396.

Bieri, M., d'Auvergne, E.J., and Gooley, P.R. (2011). relaxGUI: a new software for fast and simple NMR relaxation data analysis and calculation of ps-ns and us motion of proteins. J. Biomol. NMR *50*, 147–155.

Boehr, D.D., McElheny, D., Dyson, H.J., and Wright, P.E. (2006). The dynamic energy landscape of dihydrofolate reductase catalysis. Science *313*, 1638–1642.

Chaudhuri, B.N., Lange, S.C., Myers, R.S., Chittur, S.V., Davisson, V.J., and Smith, J.L. (2001). Crystal structure of imidazole glycerol phosphate synthase: a tunnel through the (Beta/Alpha)8 barrel joins two active sites. Structure *9*, 987–997.

Chaudhuri, B.N., Lange, S.C., Myers, R.S., Davisson, V.J., and Smith, J.L. (2003). Toward understanding the mechanism of the complex cyclization reaction catalyzed by imidazole glycerolphosphate synthase: crystal structures of a ternary complex and the free enzyme. Biochemistry *42*, 7003–7012.

Chittur, S.V., Klem, T.J., Shafer, C.M., and Davisson, V.J. (2001). Mechanism for acivicin inactivation of triad glutamine amidotransferases. Biochemistry *40*, 876–887.

Daily, M.D., and Gray, J.J. (2009). Allosteric communication occurs via networks of tertiary and quaternary motions in proteins. PLoS Comput. Biol. *5*, e1000293–e1100306.

d'Auvergne, E.J., and Gooley, P.R. (2008a). Optimisation of NMR dynamic models I. Minimisation algorithms and their performance within the model-free Brownian rotational diffusion spaces. J. Biomol. NMR *40*, 107–119.

d'Auvergne, E.J., and Gooley, P.R. (2008b). Optimisation of NMR dynamic models II. A new methodology for the dual optimisation of the model-free parameters and the Brownian rotational diffusion tensor. J. Biomol. NMR *40*, 121–133.

Delaglio, F., Grzesiek, S., Vuister, G.W., Zhu, G., Pfeifer, J., and Bax, A. (1995). NMRPipe: a multidimensional spectral processing system based on UNIX pipes. J. Biomol. NMR *6*, 277–293.

Demerdash, O.N.A., Daily, M.D., and Mitchell, J.C. (2009). Structure-based predictive models of allosteric hot spots. PLoS Comput. Biol. *5*, e1000531–e1000555.

Douangamath, A., Walker, M., Beismann-Driemeyer, S., Vega-Fernandez, M.C., Sterner, R., and Wilmanns, M. (2002). Structural evidence for ammonia tunneling across the (Beta/Alpha)8 barrel of the imidazole glycerol phosphate synthase bienzyme complex. Structure *10*, 185–193.

Fairman, J.W., Wijerathna, S.R., Ahmad, M.F., Xu, H., Nakano, R., Jha, S., Prendergast, J., Welin, R.M., Flodin, S., Roos, A., et al. (2011). Structural basis for allosteric regulation of human ribonucleotide reductase by nucleotide-induced oligomerization. Nat. Struct. Mol. Biol. *18*, 316–322.

Freiburger, L.A., Baettig, O., Sprules, T., Berghuis, A.M., Auclair, K., and Mittermaier, A.K. (2011). Competing allosteric mechanisms modulate substrate binding in a dimeric enzyme. Nat. Struct. Mol. Biol. *18*, 288–294.

Freiburger, L.A., Miletti, T., Zhu, S., Baettig, O., Berghuis, A.M., Auclair, K., and Mittermaier, A.K. (2014). Substrate-dependent switching of the allosteric binding mechanism of a dimeric enzyme. Nat. Chem. Biol. *10*, 937–942.

Goddard, T.D., and Kneller, D.G. (2008). SPARKY 3 (University of California, San Francisco).

Grey, M.J., Wang, C., and Palmer, A.G., III (2003). Disulfide bond isomerization in basic pancreatic trypsin inhibitor: multisite chemical exchange quantified by CPMG relaxation dispersion and chemical shift modeling. J. Am. Chem. Soc. *125*, 14324–14335.

Gunasekaran, K., Ma, B., and Nussinov, R. (2004). Is allostery an intrinsic property of *all* dynamic proteins? Proteins *57*, 433–443.

Hilser, V.J. (2010). An ensemble view of allostery. Science *327*, 653–654.

Hilser, V.J., Wrabl, J.O., and Motlagh, H.N. (2012). Structural and energetic basis of allostery. Annu. Rev. Biophys. *41*, 585–609.

Kimmel, J.L., and Reinhart, G.D. (2000). Reevaluation of the accepted allosteric mechanism of phosphofructokinase from *Bacillus stearothermophilus*. Proc. Natl. Acad. Sci. USA *97*, 3844–3849.

Klem, T.J., and Davisson, V.J. (1993). Imidazole glycerol phosphate synthase: the glutamine amidotransferase in histidine biosynthesis. Biochemistry *32*, 5177–5186.

Korzhnev, D.M., Kloiber, K., Kanelis, V., Tugarinov, V., and Kay, L.E. (2004a). Probing slow dynamics in high molecular weight proteins by methyl-TROSY NMR spectroscopy: application to a 723-residue enzyme. J. Am. Chem. Soc. *126*, 3964–3973.

Korzhnev, D.M., Kloiber, K., and Kay, L.E. (2004b). Multiple-quantum relaxation dispersion NMR spectroscopy probing millisecond time-scale dynamics in proteins: theory and application. J. Am. Chem. Soc. *126*, 7320–7329.

Koshland, D.E., Jr., Nemethy, G., and Filmer, D. (1966). Comparison of experimental binding data and theoretical models in proteins containing subunits. Biochemistry *5*, 365–368.

Laskowski, R.A., Gerick, F., and Thornton, J.M. (2009). The structural basis of allosteric regulation in proteins. FEBS Lett. *583*, 1692–1698.

Lipchock, J.M., and Loria, J.P. (2009). Millisecond dynamics in the allosteric enzyme imidazole glycerol phosphate synthase (IGPS) from *Thermatoga maritima*. J. Biomol. NMR *45*, 73–84.

Lipchock, J.M., and Loria, J.P. (2010). Nanometer propagation of millisecond motions in V-type allostery. Structure *18*, 1596–1607.

List, F., Vega, M.C., Razeto, A., Hager, M.C., Sterner, R., and Wilmanns, M. (2012). Catalysis uncoupling in a glutamine amidotransferase bienzyme by unblocking the glutaminase active site. Chem. Biol. *19*, 1589–1599.

Manley, G., Rivalta, I., and Loria, J.P. (2013). Solution NMR and computational methods for understanding protein allostery. J. Phys. Chem. B *117*, 3063–3073.

Massi, F., Wang, C., and Palmer, A.G., III (2006). Solution NMR and computer simulation studies of active site loop motion in triosephosphate isomerase. Biochemistry *45*, 10787–10794.

Ming, D., and Wall, M.E. (2005). Allostery in a coarse-grained model of protein dynamics. Phys. Rev. Lett. *95*, 198103–198106.

Monod, J., Wyman, J., and Changeux, J.-P. (1965). On the nature of allosteric transitions: a plausible model. J. Mol. Biol. *12*, 88–118.

Morin, S., Linnet, T., Lescanne, M., Schanda, P., Thompson, G.S., Tollinger, M., Teilum, K., Gagne, S., Marion, D., Griesinger, C., et al. (2014). Relax: the analysis of biomolecular kinetics and thermodynamics using NMR relaxation dispersion data. Bioinformatics *30*, 2219–2220.

Motlagh, H.N., Li, J., Thompson, E.B., and Hilser, V.J. (2012). Interplay between allostery and intrinsic disorder in an ensemble. Biochem. Soc. Trans. *40*, 975–980.

Motlagh, H.N., Wrabl, J.O., Li, J., and Hilser, V.J. (2014). The ensemble nature of allostery. Nature *508*, 331–339.

Myers, R.S., Jensen, J.R., Deras, I.L., Smith, J.L., and Davisson, V.J. (2003). Substrate-induced changes in the ammonia channel for imidazole glycerol phosphate synthase. Biochemistry *42*, 7013–7022.

Myers, R.S., Amaro, R.E., Luthey-Schulten, Z.A., and Davisson, V.J. (2005). Reaction coupling through interdomain contacts in imidazole glycerol phosphate synthase. Biochemistry *44*, 11974–11985.

Pervushin, K., Riek, R., Wider, G., and Wuthrich, K. (1997). Attenuated T2 relaxation by mutual cancellation of dipole-dipole coupling and chemical shift anisotropy indicates an avenue to NMR structures of very large biological macromolecules in solution. Proc. Natl. Acad. Sci. USA *94*, 12366–12371.

Popovych, N., Sun, S., Ebright, R.H., and Kalodimos, C.G. (2006). Dynamically driven protein allostery. Nat. Struct. Mol. Biol. *13*, 831–838.

Popovych, N., Tzeng, S.-R., Tonelli, M., Ebright, R.H., and Kalodimos, C.G. (2009). Structural basis for cAMP-mediated allosteric control of the catabolite activator protein. Proc. Natl. Acad. Sci. USA *106*, 6927–6932.

Rivalta, I., Sultan, M.M., Lee, N.S., Manley, G., Loria, J.P., and Batista, V.S. (2012). Allosteric pathways in imidazole glycerol phosphate synthase. Proc. Natl. Acad. Sci. USA *109*, E1428–E1436.

Rousseau, F., and Schymkowitz, J.A. (2005). A systems biology perspective on protein structural dynamics and signal transduction. Curr. Opin. Struct. Biol. *15*, 23–30.

Scott, D.W. (1979). On optimal and data-based histograms. Biometrika *66*, 605–610.

Sinha, S.C., Chaudhuri, B.N., Burgner, J.W., Yakovleva, G., Davisson, V.J., and Smith, J.L. (2004). Crystal structure of imidazole glycerol-phosphate dehydratase: duplication of an unusual fold. J. Biol. Chem. *279*, 15491–15498.

Tsai, C.-J., and Nussinov, R. (2014). A unified view of "how allostery works". PLoS Comput. Biol. *10*, 1–12.

Tugarinov, V., and Kay, L.E. (2004). An isotope labeling strategy for methyl TROSY spectroscopy. J. Biomol. NMR *28*, 165–172.

Tzeng, S.-R., and Kalodimos, C.G. (2009). Dynamic activation of an allosteric regulatory protein. Nature *462*, 368–372.

Vanwart, A., Eargle, J., Luthey-Schulten, Z.A., and Amaro, R.E. (2012). Exploring residue component contributions to dynamical network models of allostery. J. Chem. Theory Comput. *8*, 2949–2961.

Velyvis, A., Schachman, H.K., and Kay, L.E. (2009). Application of methyl-TROSY NMR to test allosteric models describing effects of nucleotide binding to aspartate transcarbamoylase. J. Mol. Biol. *387*, 540–547.

Wolfenden, R., and Snider, M.J. (2001). The depth of chemical time and the power of enzymes as catalysts. Acc. Chem. Res. *34*, 938–945.